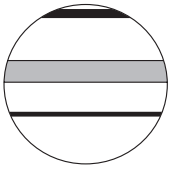

Research paper

The Holocene
2018, Vol. 28(11) 1731–1744

DOI: 10.1177/0959683618788701
journals.sagepub.com/home/hol

A 2000-year record of ocean influence on Jakobshavn Isbræ calving activity, based on marine sediment cores

David J Wangner,[1,2] Anne E Jennings,[3] Flor Vermassen,[1,2] Laurence M Dyke,[1] Kelly A Hogan,[4] Sabine Schmidt,[5] Kurt H Kjær,[2] Mads F Knudsen[6] and Camilla S Andresen[1]

Abstract

The Greenland Ice Sheet has experienced significant mass loss in recent years. A substantial component of this is attributable to the retreat of marine-terminating outlet glaciers, which lose mass through increases in calving, submarine melting and terrestrial meltwater discharge. In terms of iceberg production, Jakobshavn Isbræ is the largest marine-terminating glacier in Greenland, yet relatively little is known about its history before the first glacier margin observations in 1851. Two marine sediment cores obtained 15 and 19 km northwest from the mouth of Jakobshavn Isfjord were analysed to reconstruct the past behaviour of Jakobshavn Isbræ and to investigate the response of the glacier system to ocean forcing. These records provide long-term (~2000) context for assessing the significance of the rapid changes in glacier stability over the last century. The X-ray imagery and high-resolution grain size analysis from both cores reveal distinct multi-centennial-scale changes in the flux of iceberg-rafted debris (IRD) from Jakobshavn Isbræ. Foraminiferal analysis shows that variability in the relatively warm West Greenland Current (WGC) may have been an important driver of calving activity at Jakobshavn Isbræ. We find that iceberg rafting and WGC inflow were relatively high from onset of the record, at 60 BC, until AD 1100. Subsequently, the inflow of the WGC into Disko Bugt decreased. This was accompanied by a dramatic reduction in IRD from AD 1500 to 1850, which is attributed to the establishment of a floating ice tongue. We also show that ocean warming in the 20th century is part of a longer-term warming trend in the WGC which started at around AD 1700. Finally, these new records underline the complexity of glaciomarine sediments; IRD variability was driven by the inflow of the WGC but was also modulated by a complex interplay of air temperature, sea-ice coverage and ice margin proximity.

Keywords

Disko Bugt, foraminifera, Greenland, Holocene, ice-rafted debris, Jakobshavn Isbræ, palaeoclimatology, West Greenland Current

Received 13 March 2018; revised manuscript accepted 9 June 2018

Introduction

Measurements and observations of volumetric changes of the Greenland Ice Sheet (GrIS) have improved significantly over the past two centuries. The first glacier observations and temperature measurements were obtained in the late 18th century (Box, 2002; Box et al., 2009; Joughin et al., 2004; McMillan et al., 2016; Vinther et al., 2006). The advent of satellite imaging in the late 1970s and subsequent advances in radar altimetry, laser altimetry and gravimetric monitoring have led to substantial improvements in our understanding of the magnitude and causes of mass loss (Chen et al., 2006; Pritchard et al., 2009; Shepherd et al., 2012). The GrIS has experienced a dramatic decrease in the total mass balance since the beginning of the 20th century, which has included rapid retreat of the majority of marine-terminating glaciers around Greenland (Alley et al., 2010; Box and Colgan, 2013; Kjeldsen et al., 2015; Weidick and Bennike, 2007). Given the vast quantities of freshwater release associated with glacier instability, an improved understanding of the processes of ice-sheet change, and the underlying forcing mechanisms, is crucial for improving future predictions of global sea-level rise and changes in the thermohaline circulation in the North Atlantic (Holland et al., 2008; Straneo et al., 2013). Oceanic and atmospheric warming are thought to be primary drivers of marine-terminating glacier retreat in Greenland (Andresen et al., 2012b; Holland et al., 2008; Rignot et al., 2012; Straneo et al., 2011). However, further data linking oceanographic and glacio-dynamic processes are required to better understand the physical processes and their evolution at longer timescales than are available from instrumental records (Straneo and Heimbach, 2013). Furthermore, individual glaciers often exhibit unique responses to changes in external forcing and it is therefore crucial to study glaciers across a wide variety of physical settings (Carr and Hiemstra, 2013; Enderlin et al., 2013).

Geological records can be used to reconstruct past environmental conditions beyond instrumental records and provide valuable empirical data for understanding how the GrIS responds to

[1]Department of Glaciology and Climate, Geological Survey of Denmark and Greenland (GEUS), Denmark
[2]Centre for GeoGenetics, Natural History Museum, University of Copenhagen, Denmark
[3]INSTAAR and Department of Geological Sciences, University of Colorado Boulder, USA
[4]British Antarctic Survey, UK
[5]UMR 5805 EPOC, University of Bordeaux, France
[6]Department of Earth Sciences, University of Aarhus, Denmark

Corresponding author:
David J Wangner, Department of Glaciology and Climate, Geological Survey of Denmark and Greenland (GEUS), Øster Voldgade 10, DK-1350 Copenhagen K, Denmark.
Email: dawangner@gmail.com

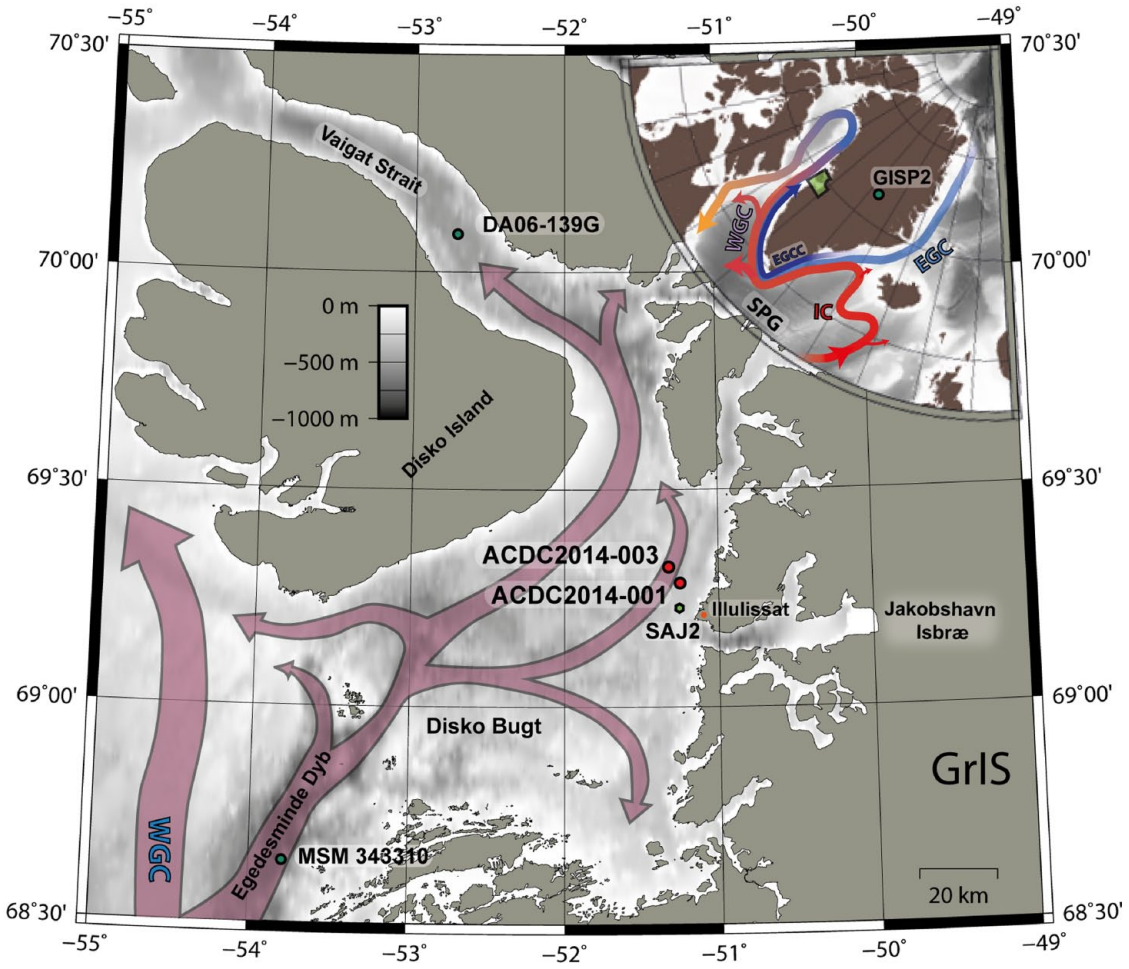

Figure 1. Map of Disko Bugt area with core locations indicated by red dots and other stations mentioned in the text by green dots. Main pathways of the West Greenland Current (WGC) are shown with red arrows (adapted from Ribergaard et al., 2006). Inset map shows Greenland and major surface ocean currents (Straneo et al., 2012). East Greenland Current (EGC), Irminger Current (IC), East Greenland Coastal Current (EGCC) and West Greenland Current (WGC) south of Greenland the IC forms the Subpolar Gyre (SPG). Bathymetric data are from the IBCAO v3 (Jakobsson et al., 2012). The figure was produced using GMT (Wessel et al., 2013).

atmospheric and oceanographic changes. Long-term reconstructions of glacier behaviour also provide context for assessing the magnitude, frequency and duration of recent changes. Here, we extend the record of glaciological change and oceanic variability at Jakobshavn Isbræ two millennia back in time by analysing marine sediment cores from Disko Bugt (Figure 1). Oceanographic variability is reconstructed from benthic foraminifera assemblages. Glaciological behaviour is tracked by measuring the abundance of iceberg-rafted debris (IRD) originating from Jakobshavn Isbræ. We combine these records to assess the stability of Jakobshavn Isbræ in response to oceanic and climatic forcing through the late Holocene.

Study area

Disko Bugt is a ~40,000 km^2 embayment in West Greenland (Figure 1). The bay is generally 200 to 400-m deep, but maximum water depths of ~1100 m b.s.l. are found in Egedesminde Dyb (Hogan et al., 2012). The oceanography in Disko Bugt is dominated by the inflow of a branch of the West Greenland Current (WGC). The WGC is formed by the mixing and coupling of the Irminger Current (IC) and the East Greenland Current (EGC) as they flow northwards along the coast of southwest Greenland (Ribergaard et al., 2006). The IC brings relatively warm, saline water sourced from the North Atlantic Current, whereas the EGC bears cold and relatively fresh water from the Arctic Ocean (Figure 1). The two individual water masses are distinguishable within Disko Bugt. The IC component, which forms the bottom water in Disko Bugt, is characterised by temperatures of 2.5–3.5 °C and salinities between 32.5 and 34.8 psu. Intermediate waters are derived from the EGC and are typically characterised by temperatures between 1 and 3 °C and salinities of 32–33.7 psu (Andersen, 1981; Beaird et al., 2017). The WGC enters Disko Bugt from the southwest and exits the bay primarily through Vaigat Strait in the north (Ribergaard et al., 2006). Surface waters (0–50 m b.s.l.) are cold and fresh (−1 to 0°C and down to 25 psu), which reflects the influence of sea ice, icebergs and meltwater from the multiple glacier outlets that drain into the bay (Beaird et al., 2017).

Jakobshavn Isbræ

Jakobshavn Isbræ is the largest marine-terminating glacier in West Greenland; it drains around 7% of the GrIS (Bindschadler, 1984) and discharges ~24 km^3 of ice annually; it is responsible for ~10% of the iceberg production in Greenland (Rignot and Kanagaratnam, 2006; Weidick and Bennike, 2007). Consequently, Jakobshavn Isbræ is by far the largest contributor to current mass loss in Greenland (Enderlin et al., 2014; van den Broeke et al., 2016). Ice-penetrating radar has identified a large palaeo-fluvial drainage basin underneath the ice sheet which covers about 20% of the total land area of Greenland (Bamber et al., 2013; Cooper et al., 2016). The ice stream drains into Disko Bugt via this drainage system and into the 45-km-long Ilulissat Fjord; the fjord is ~4-km wide at the fjord mouth and has water depths down to 1000 m b.s.l. (Schumann et al., 2012; Weidick and Bennike, 2007). The fjord shallows to 200 m b.s.l. at the mouth where a prominent sill hinders iceberg

release (Schumann et al., 2012). Previous studies of the Holocene in Disko Bugt, Egedesminde Dyb and Vaigat Strait have focused on palaeo-oceanographic variability (Krawczyk et al., 2013, 2016; Moros et al., 2016; Ouellet-Bernier et al., 2014; Perner et al., 2011; Ribeiro et al., 2012; Sha et al., 2014; Sheldon et al., 2015) and in some cases also glaciological changes (Andresen et al., 2011; Lloyd et al., 2006a, 2011). The glaciological changes at Jakobshavn Isbræ have also been reconstructed from a land-based perspective using threshold lakes as well as from mapping and dating glacial landforms (Briner et al., 2010; Corbett et al., 2011; Kelley et al., 2013; Weidick and Bennike, 2007; Young et al., 2011). To summarise, these result show that after 7300–7600 yr BP, the terminus of Jakobshavn Isbræ was behind its current position (Briner et al., 2010; Corbett et al., 2011; Weidick and Bennike, 2007).

Based on lake sediments from Iceboom Lake north of Ilulissat Fjord, Young et al. (2011) suggest that the land-based ice margin advanced beyond its present-day configuration between AD 1500 and AD 1640 and 1850. However, for the region south of Jakobshavn Isbræ, Briner et al. (2010) dated the advance to 350 BC (1900 years earlier). Based on the same lake cores, Briner et al. (2011) suggest a rapid response of Jakobshavn Isbræ on the 'Little Ice Age' (LIA) cooling and a late advance of the glacier terminus 'at least after AD ~1650 to ~1700, and more likely AD ~1800'.

Since the middle of the 19th century, it has been possible to directly reconstruct the behaviour of Jakobshavn Isbræ from historical observations, aerial photographs and satellite imagery (Csatho et al., 2008; Kjeldsen et al., 2015; Weidick and Bennike, 2007). The results from Csatho et al. (2008) show three periods of rapid thinning since the end of the 'LIA'; these occurred from 1902–1913, 1930–1959 and has been especially pronounced from 1999 to the present day.

Materials and methods

Sampling design

Two sediment cores were collected in August 2014 from *R/V Porsild* using a Rumohr corer equipped with 2-m core liners (Meischner and Rumohr, 1974). This type of coring device ensures that the core top is preserved intact. The core locations are 15–19 km northwest of the mouth of Jakobshavn Isfjord in water depths between 380 and 391 m and are approximately spaced 4 km apart (Figure 1, Table 1). As prevailing currents flow northwards, these locations were chosen to catch the sediment and iceberg flux exiting the fjord.

Table 1. Coordinates of core sites and recovery.

Core ID	Latitude	Longitude	Water depth (m)	Length (cm)
ACDC2014-001	69 N 17,20′	51 W 16,20′	391	162
ACDC2014-003	69 N 18,78′	51 W 19,83′	380	173

Core imaging

The X-ray images were produced with a *YXLON smart 160E/0.4 system* at the National Museum of Denmark, Copenhagen (120 s, 3 mA, 90 KV). Single images, covering approximately 40 cm of the core half, were merged manually using *Gimp 2.8* software to produce a composite X-ray image of the entire core. Line scans of each core were obtained using an *Itrax Core scanner* at the Natural History Museum of Denmark. Contrast and brightness were increased using *Photoshop CS6*.

Sediment grain size analysis

Grain size analyses were undertaken on both cores (ACDC2014-001 and ACDC2014-003) by wet sieving through 63 and 150 µm *Retsche* sieves. Material for the grain size analyses was sampled continuously throughout the cores at 1-cm increments. Samples were weighed before and after freeze-drying to determine the water content. Dry sample weights ranged from 3 to 11 g. Grains heavier than 0.1 g were manually picked from the >150-µm fraction, weighed and following excluded from further calculations to avoid the disproportional impact of single grains. Laser diffraction measurements were performed on the <63-µm grain size fraction. Measurements were undertaken using a *Malvern Mastersizer 3000*. Between 65 and 90 mg of the samples were homogenised in an agate mortar and put in a test tube. Samples were then dispensed with 15-mL 0.005 M tetra-sodium-diphosphate-decahydrate, and the solution was treated with an ultrasound probe for 45 s.

Fluxes (F) of the >150-µm fraction were calculated with the formula:

$$F = \frac{S}{W} \times P \times d$$

where F is the fluxes $(\mathrm{kg/m^2 \times yr})$, S is the sedimentation rate $(\mathrm{m/yr})$, W is the water content, P is the weight percentage of the >150 fraction and d is the density of quartz $(2700\,\mathrm{kg/m^3})$.

Foraminiferal assemblage analysis

Foraminiferal assemblage analysis was undertaken on 1-cm slices of sediment every 5 cm within core ACDC2014-001. Eight additional samples were analysed between 82 and 127 cm. As both cores show a similar stratigraphy, the analysis was focused on one core only. Samples were soaked overnight in a solution of sodium metaphosphate before sieving at 63 µm. Samples were stored in a solution (targeted pH ~8) of distilled water, ethanol and sodium bicarbonate to avoid carbonate dissolution (Lloyd et al., 2005). Samples with high foraminifera concentrations were split into eighths using a wet splitter. Where possible, a minimum of 300 specimens were identified and counted on a picking tray. However, low concentrations of foraminifera between 97 and 107 cm only allowed a count of 51 and 94 specimens, respectively, despite using the full sample. Additional samples containing less than 300 specimens were obtained between 85 and 90 cm and at 157 cm. Data were plotted using the software *C2* (Juggins, 2007). For statistical analyses, species >2% were fed into the software *PAST* (Hammer et al., 2001) to run a principal component analyses (PCAs). The PCA of the percentage data was run with square root transform. PCA case scores versus depth and PCA variable loadings for each species were calculated (Figure 2 and 4). Furthermore, a constrained cluster analysis was run with a paired group algorithm and a Euclidean similarity measure.

Chronological constraint

The age of sediments in cores ACDC2014-001 and ACDC2014-003 was constrained with lead-210 (^{210}Pb) and carbon-14 (^{14}C) age determinations. The lead-210 dating is based on the reduction in excess ^{210}Pb ($^{210}Pb_{xs}$) in the sediment. In practice, aliquots of bulk sediment were taken within the upper 30 cm in a 5 cm resolution to measure the ^{210}Pb, ^{226}Ra and ^{137}Cs activities using a low-background, high-efficiency gamma detector (Supplementary Figure 1, available online). Excesses of ^{210}Pb were calculated as the difference of the measured ^{210}Pb and ^{226}Ra activities. Radiocarbon dating was undertaken on 15 samples of seaweed using accelerator mass spectrometry (AMS). Seven samples were prepared at the Laboratory for AMS Radiocarbon Preparation and Research (INSTAAR, University of Colorado, Boulder, CO, US), four samples at Beta Analytic (Miami, FL, US) and four samples at Lund University (Lund, Sweden).

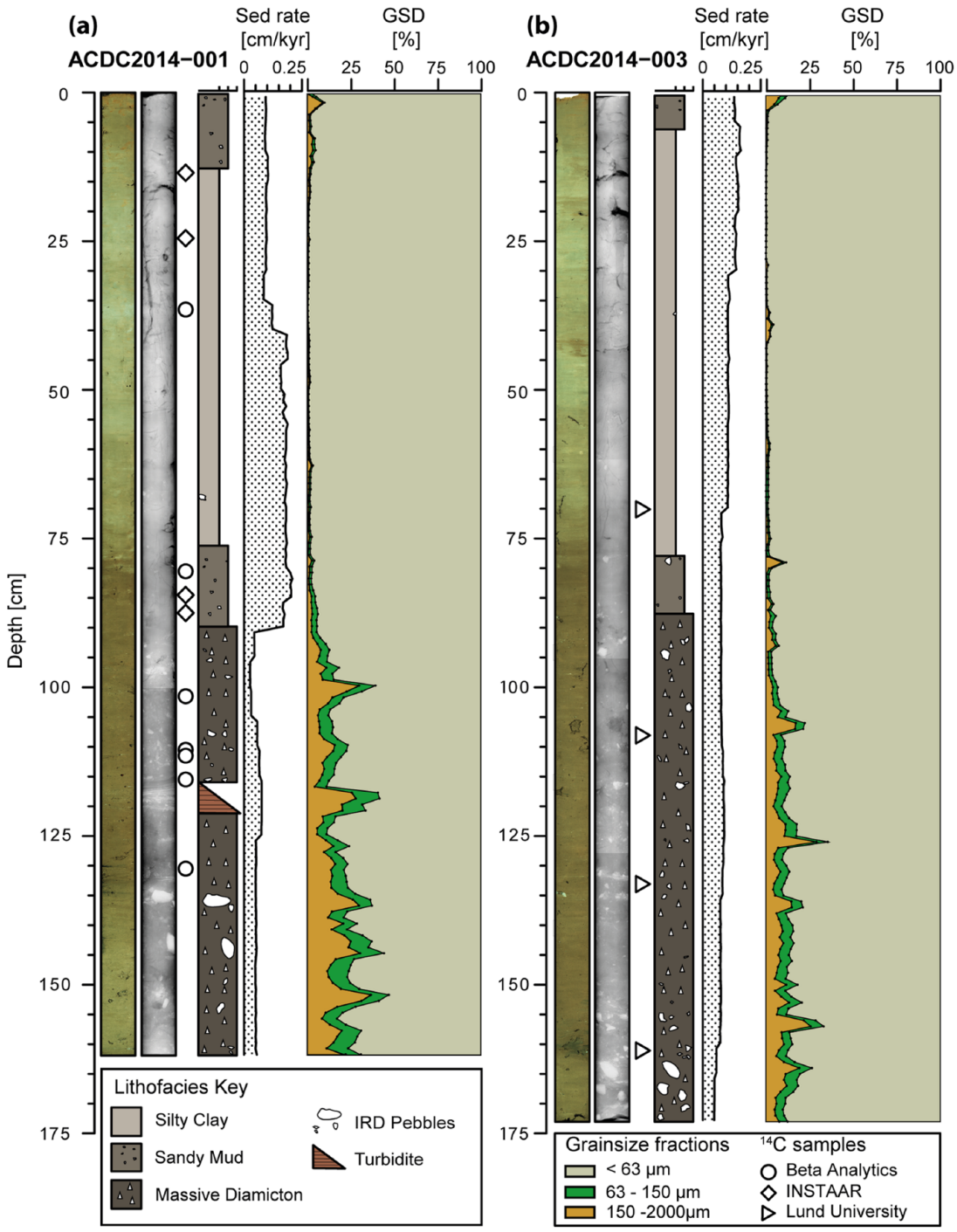

Figure 2. Core descriptions for (a) ACDC2014-001 and (b) ACDC2014-003. From left to right: Line scan with increased contrast and brightness. Composite X-ray images. Location of radiocarbon dates is indicated by white circles (INSTAAR), squares (Beta Analytic) and triangles (University of Lund). Lithofacies identified in the core. Sedimentation rates calculated from the age model. The coloured summary plot shows the grain size distribution (GSD) at 1-cm resolution, orange = 150 µm–2 mm, green = 63–150 µm, grey = <63 µm.

Time series analysis

The spectral properties of the grain size data from sediment cores ACDC2014-001 and ACDC2014-003 were analysed using the Lomb–Scargle Fourier transform (Lomb, 1976; Scargle, 1982). This method is directly applicable to unevenly spaced data. The grain size records were first detrended with a polynomial of degree 5 to suppress spectral leakage from the low-frequency harmonics. Subsequently, the data were grouped in overlapping 1000 year windows, with a spacing of 20 years. Next, the spectrum and associated red-noise (AR1) false-alarm levels were computed for all individual windows. The univariate spectra were bias-corrected using 1000 Monte Carlo simulations, based on the publicly available software package REDFIT (Schulz and Mudelsee, 2002), which automatically produces first-order autoregressive (AR1) time series with sampling times and characteristic timescales matching the measured data. This approach makes it possible to assess the statistical significance of the spectral peaks that are mapped and coloured according to their significance in the time-dependent spectral density plots (Supplementary Figure 2, available online).

Results

Sedimentology

The sediment in both cores consists of dark olive to olive-grey mud (Munsell colour code: 5Y/1, the contrast of pictures in Figure 2 is increased to show variations). The processed colour

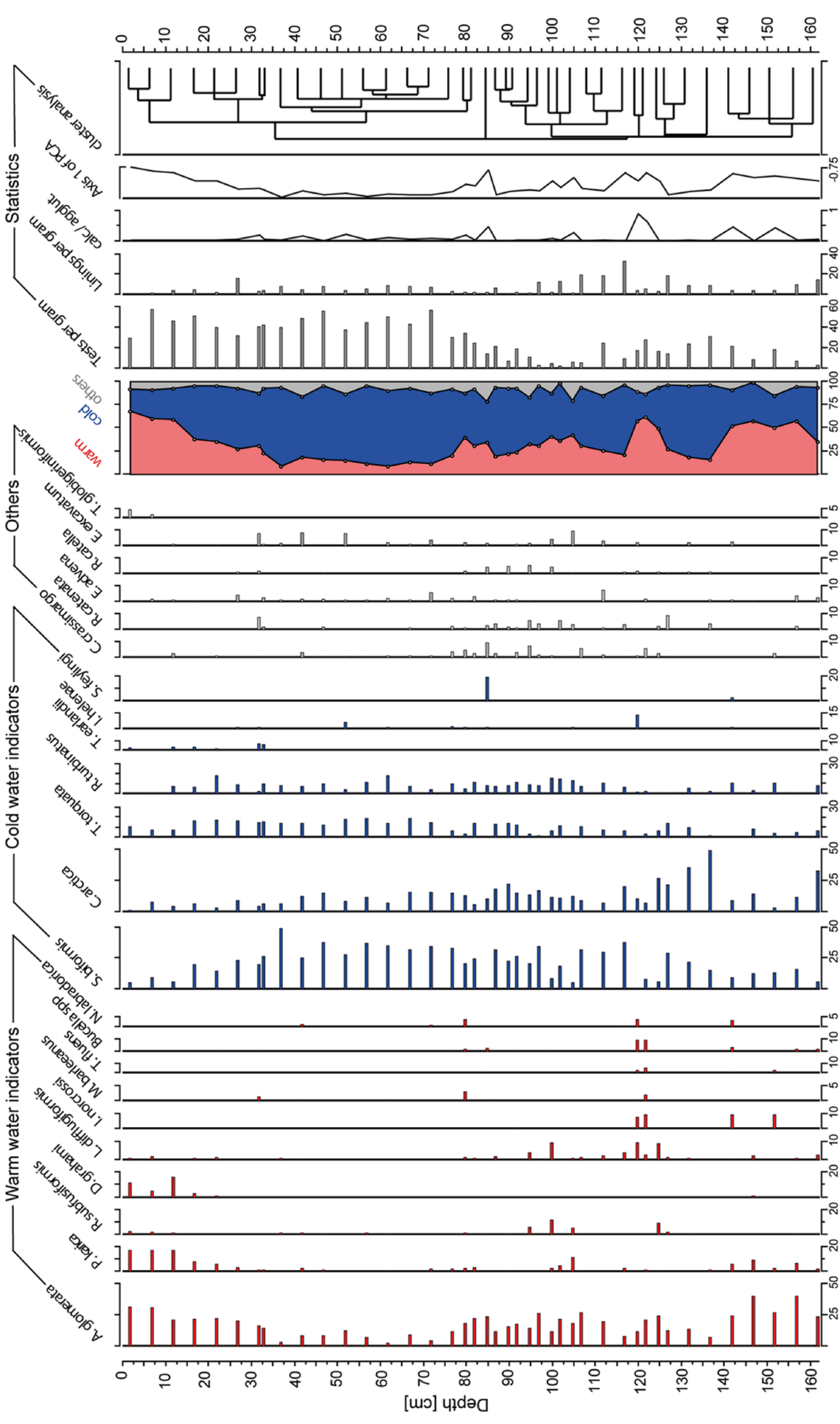

Figure 3. Agglutinated and calcareous species in core ACDC2014-001. The turbidite section between 121 to 117 cm is excluded from the data. Foraminiferal abundances are expressed as a percentage of total specimens counted. Species are grouped into cold water indicators (blue), warm water indicators (red) and undefined (grey). Stacked indicators are from both agglutinated and calcareous species. Concentrations are of foraminifera and test linings. Statistics is derived from the PCA with 'past' (Hammer et al., 2001).

scan reveals slightly darker sediments in the upper 10 cm, a lighter interval between 10 and 75 cm and a darker interval below 75 cm in both cores.

In core ACDC2014-001, the sediment lightens slightly again below 135 cm, whereas in core ACDC2014-003, the sediment lightens below 160 cm.

ACDC2014-001. Visual core descriptions and the X-ray images reveal that the sediment from 152 to 85 cm is characterised by a massive matrix-supported diamicton unit with a high abundance of sub-angular gravel throughout and larger, slightly rounded pebbles at 135 and 142 cm. In the work by Streuff et al. (2017), a similar unit was described as a 'matrix-supported diamict with a mud-dominated matrix' (their LD5). A coarse section from 121 to 117 cm shows characteristics indicative of a turbidite deposit (erosive base and an upwards fining trend) and is consequently excluded from further analysis.

The upper 85 cm of the core consists of homogeneous, structureless, silty clay with almost no sand and gravel content (Figure 2). This part of the core corresponds to the lithofacies LD2c in Streuff et al. (2017), where it is described as 'massive, occasionally bioturbated mud' It was found in multiple cores (JR175-VC05, VC06 and VC10) 15 to 35 km west of Ilulissat Fjord.

Grain size is highly variable throughout the core and can be divided into the following sections.

The bottom of the core, up to 90 cm, shows relatively high values in the sand fraction (>63 μm) with an average of ~20 wt%. The signal is highly variable with major peaks at 100, 119, 137, 145 and 152 cm. The grain size gradually increases from 90 to 77 cm into an interval from 77 to 20 cm consisting of silty clay with a sand content of less than 1 wt%. The uppermost 20 cm of the core contains small amounts of sand, with an average of 2.86 wt%.

ACDC2014-003. The X-ray images show a sediment structure that is similar to core ACDC2014-001. Below 90 cm, the sediment consists of a matrix-supported diamicton with several sub-angular pebble-sized clasts at 95, 117 and below 155 cm. This transitions into a homogeneous, structureless mud with very low percentages of sand and occasional larger clasts.

The similarity with ACDC2014-001 is also reflected in the grain size composition. Between 173 and 100 cm, the sand fraction of core ACDC2014-003 shows a high variability with peaks at 106, 126, 136, 156 and 164 cm and an average of ~14 wt%. Above 100 cm, the grain size gradually decreases to a fine-grained silty clay with minor peaks at 80 cm, 40 cm and in the uppermost 2 cm. The mean sand content in this interval is ~2 wt%. The variability in grain size is mostly shaped by an increase in the >150-μm fraction, whereas the 63- to 150-μm fractions stay relatively constant (4–8 wt%); this pattern is also observed in core ACDC2014-001.

Foraminiferal assemblages

In total, 33 different species were found during the foraminifera assemblage analyses (17 agglutinated and 16 calcareous). A complete list of species can be found in the supplementary information. One single planktonic test, *Neogloboquadrina pachyderma*, was found at 33 cm depth; this was not included in the percentage calculations. Results presented here are based on benthic foraminifera only. The assemblages for agglutinated and calcareous species are shown together in Figure 2. Percentages were calculated relative to the total count (Jennings et al., 2002). Species were divided into three categories: warm water indicators (WWIs), cold water indicators (CWIs) and others. Species were assigned to these categories on the basis of their environmental preferences established from previous research in the region (Jennings et al., 2017; Lloyd, 2006a, 2006b; Sheldon et al., 2016). Furthermore, species that were not attributed to any preference in former literature but showed strong correlation with other species based on the PCA were also added into these categories.

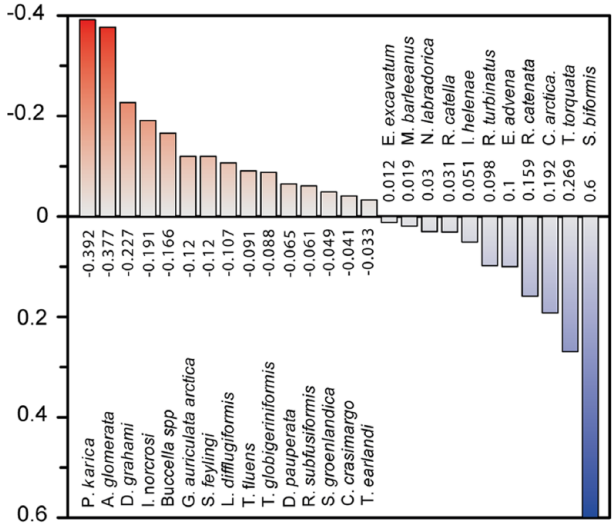

Figure 4. Loadings on Axis 1 derived from the principal component analysis. Only species with an abundance >2% were included in this analysis. PCA analysis was undertaken using PAST software (Hammer et al., 2001).

The species *Adercotryma glomerata, Portatrochammina karica* (formerly *Portatrochammina bipolaris*), *Reophax subfusiformis, Trifarina fluens, Buccella* spp, *Melonis barleeanus* and *Nonionellina labradorica* are commonly associated with Atlantic water inflow in the Disko Bugt region and thus are considered to be WWIs in this study (Lloyd, 2006a; Lloyd et al., 2007; Perner et al., 2013; Sheldon et al., 2016). We note that Lloyd et al. (2006a, 2007) used *Islandiella norcrossi* as a cold Arctic water indicator but this species has also been used as a WWI for areas slightly further offshore in this region (Perner et al., 2011, 2013). Thus, *I. norcrossi* was included in the WWI group. *Deuterammina grahami* has not been described in previous Disko Bugt studies but strongly correlates with WWIs and was therefore included in the WWI category (Figure 4).

Spiroplectammina biformis, Cuneata arctica, Textularia torquata, Recurvoides turbinatus, Islandiella helenae and *Stainforthia feylingi* are associated with cold Arctic water. Although the PCA analyses reveal a negative value for *Textularia earlandi* and *S. feylingi*, they are both included in the CWI group (Figure 4).

The foraminiferal assemblages are dominated by agglutinated species. Calcareous species do not show a continuous occurrence but are present in increased abundances within single samples. The lowest part of the core is dominated by *A. glomerata*. The samples at 152 and 142 cm show relatively high amounts of calcareous species. At 140–127 cm, there is an increase in CWI mostly because of an increase in *C. arctica*, to a maximum of 61%. The samples at 122 and 120 cm show a relatively high abundance of calcareous species in general (*I. helenae, I. norcrossi* and *T. fluens*) and a strong increase in WWI species. Between 117 and 80 cm, the prevalence of WWIs decreases with a concomitant increase in CWIs. From 80 to 35 cm, the assemblages are characterised by the lowest abundance of WWI (13%) and a concurrent increase in CWI species (77%); this interval is mostly dominated by a high abundance of *S. biformis*. Calcareous species, mostly *I. helenae* and *Elphidium excavatum*, are not very abundant but are found occasionally. The upper 35 cm of the core is characterised by a marked increase in WWI, especially *A. glomerata, P. karica* and *D. grahami*. Calcareous species were rarely found in this part of the core.

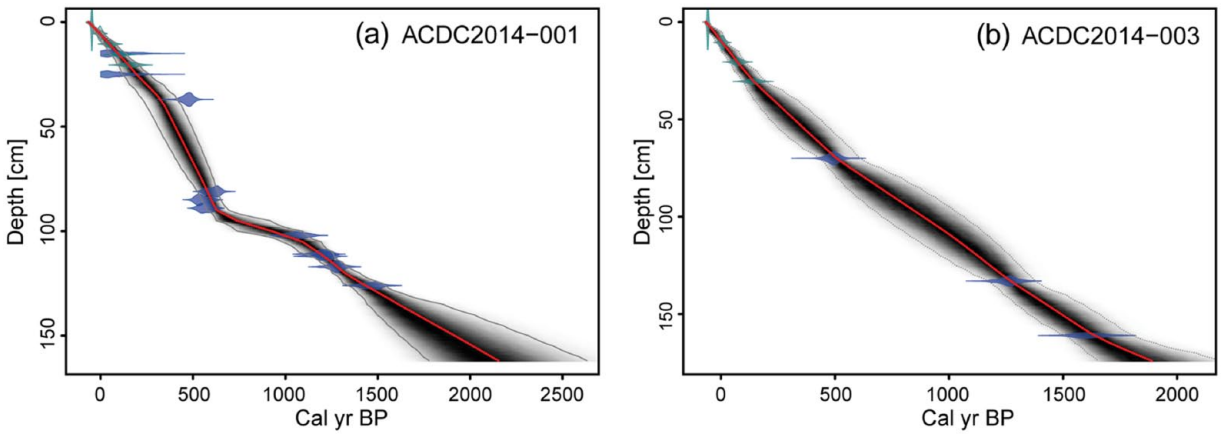

Figure 5. Age models for core (a) ACDC2014-001 and (b) ACDC2014-003. Calibrated radiocarbon samples are shown in blue and ^{210}Pb samples in green. The red line indicates the used ages and the grey shade is the 95% certainty range. The program automatically excluded sample ACDC2014-003_108.

Table 2. Radiocarbon and ^{210}Pb dating results of core ACDC2014-001.

Radiocarbon measurements					^{210}Pb dating			
Depth (cm)	Lab ID	^{14}C age (cal. yr BP)	Error ±	Calibrated age (cal. yr BP)	Depth (cm)	Excess ^{210}Pb	Calculated age (years)	Error ±
15	Beta-431618	Modern			1.5	85.4 ± 5.0	16.6	2.5
25	Beta-431617	Modern			5.5	45.8 ± 4.2	60.7	9.1
37	#-31834	845	±30	355	10.5	17.5 ± 3.0	115.9	17.3
81	#-31835	1045	±30	516	15.5	2.7 ± 2.6	171.0	25.5
85	Beta-431619	950	±30	447	20.5	0.1 ± 2.5	226.2	33.7
89	Beta-431620	980	±30	471	30.5	−0.9 ± 2.2		
102	#-31836	1515	±30	922				
111	#-31837	1640	±30	1052				
112	#-31838	1650	±30	1064				
117	#-31839	1725	±30	1148				
126	#-31840	1925	±30	1330				

Table 3. Radiocarbon and ^{210}Pb dating results of core ACDC2014-003.

Radiocarbon measurements					^{210}Pb dating			
Depth (cm)	Lab ID	^{14}C age (cal. yr BP)	Error ±	Calibrated age (cal. yr BP)	Depth (cm)	Excess ^{210}Pb	Calculated age (years)	Error ±
70	003_70	875	35	377	1.00	101.4 ± 8.7	6.9	0.7
108	003_108	3435	45	3130	5.50	55.5 ± 5.7	38.2	4.1
133	003_133	1710	45	1129	10.50	18.6 ± 3.6	73.0	7.8
161	003_161	2040	35	1447	15.50	> 1.5	107.7	11.4
					20.50	1.6 ± 2.6	142.5	15.1

The number of foraminifera found per gram of wet sediment changes within the core. Around 10 tests per gram were counted in the lower half of the core. However, above 85 cm, numbers of foraminifera increase to around 60 tests per gram average. Below 85 cm, the decrease in tests is accompanied by an increase in counted test linings. This suggests some dissolution of calcium carbonate tests. The cluster analysis confirms the separation of the core into two main assemblage regimes at 85 cm.

Age modelling

The age models for cores ACDC2014-001 and ACDC2014-003 were produced by combining the results of ^{210}Pb and ^{14}C dating (Figure 5). The CF/CS (constant flux, constant sedimentation) model was applied for age determination based on the $^{210}Pb_{xs}$ profile. All data points (Tables 2 and 3) were then fed into the software *Bacon* in R (Blaauw and Christen, 2011). Radiocarbon ages were calibrated using the *Marine13* calibration curve (Reimer et al., 2013) a ΔR of 140 ± 35 (Perner et al., 2011). In the upper part of core ACDC2014-001, the results from ^{210}Pb and ^{14}C dating are contradictory, as the ^{14}C determinations are much younger than the ^{210}Pb results. Both cores show a relatively regular (logarithmic) decay in their ^{210}Pb profiles, which strengthens the confidence in the in ^{210}Pb age model within the top 20 cm. In addition, only sediments corresponding to sediments deposited since 1950 show detectable levels of ^{137}Cs (Supplementary Figure 1, available online).

For core ACDC2014-003, the ^{210}Pb dating and three radiocarbon dates were taken into account, whereas the sample from 108 cm is excluded from the age model as the measured radiocarbon age (3435 yr BP) indicates reworking of the plant material.

Discussion

Oceanographic changes in Disko Bugt

There are multiple factors influencing the structure of foraminiferal assemblages in marine sediments. Foraminifera assemblage data

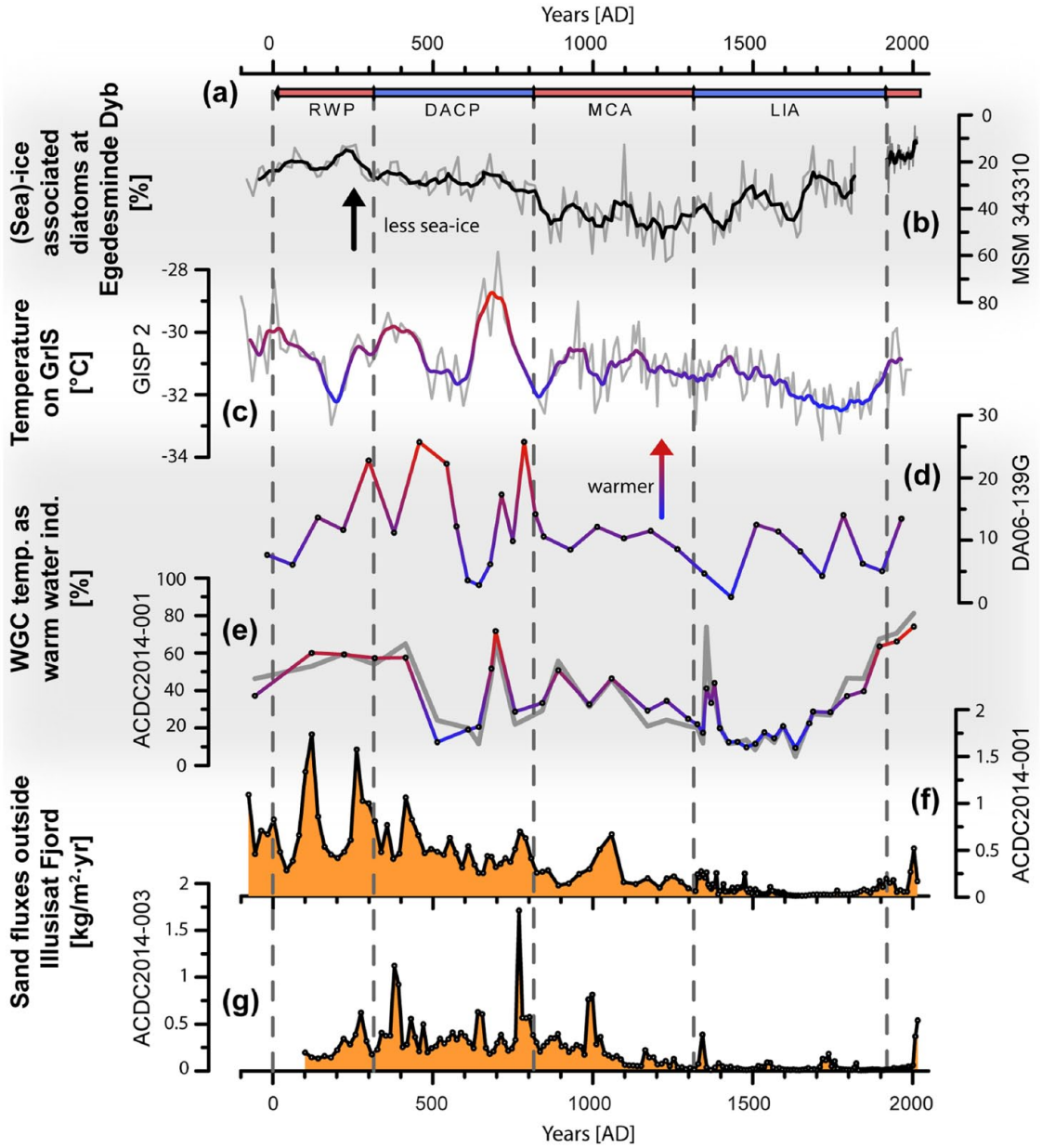

Figure 6. Records of ocean, climate and glacier behaviour in the late Holocene. (a) European climate intervals as defined in Ljungqvist (2010), (b) reconstructed sea ice coverage in outer Disko Bugt/Egedesminde Dyb (Krawczyk et al., 2013). The black line shows a 5-point running mean. Note the inverted y-axis. (c) Reconstructed surface temperature at the GISP2 ice core location (Kobashi et al., 2011). The thick line shows the 59-point running mean. (d) Atlantic water foraminiferal assemblage from Vaigat Strait (Andresen et al., 2011). Data are plotted versus an updated age model according to Sha et al. (2014). (e) Warm water indicators as percentage of the total assemblage (this study). The grey line represents Axis 1 of the PCA. (f) and (g) Results of the grain size analyses from core (f) ACDC2014-001 and (g) ACDC2014-003. Shown data are the calculated fluxes of the 150- to 2000-µm fraction (this study).

have been widely used to infer the temperature of bottom waters in high-latitude environments (Jennings and Weiner, 1996; Lloyd et al., 2011; Perner et al., 2013; Sheldon et al., 2015). However, foraminifera assemblages may also be controlled by salinity, water depth, nutrient supply and the substrate of the sediment. According to Lloyd (2006b), salinity and water depth are the most important variables in Disko Bugt; sediment substrate provides a secondary control, and bottom water temperature, total organic carbon and total nitrogen are less important. However, the correlation between temperature and foraminiferal assemblage variability has been shown in multiple studies comparing foraminifera assemblages with instrumental records (Jennings and Helgadottir, 1994; Lloyd et al., 2011; Perner et al., 2013). Ocean temperatures in Disko Bugt are primarily controlled by the strength of the WGC which, in turn, is controlled by the relative strengths of IC and EGC (Myers et al., 2007; Straneo et al., 2012). Furthermore, meltwater from the melting of icebergs and subglacial discharge can also influence the temperature of the water at the core location. However, glacially modified water forms a thick, stratified layer down to 125 m b.s.l. in coastal areas and consequently this water mass does not directly influence the bottom waters at the core sites (380 and 391 m b.s.l.) (Beaird et al., 2017). We use the relative variability in foraminiferal assemblage data as a proxy for temperature at the seabed. As this is controlled by the incursion of the WGC it represents a proxy for remote oceanographic changes (e.g. Krawczyk et al., 2016; Lloyd, 2006a; Perner et al., 2011). Figure 6e shows the percentage of WWIs superimposed on the PCA scores on Axis 1. This axis explains 23% of the variation in the assemblages (Eigenvalue: 4.415). The clear correlation strengthens the interpretation of Axis 1 as a representation of warm–cold species.

The cluster analyses of the foraminiferal assemblage data (Figure 2) indicate a clear change in the assemblage at 85 cm,

which represents the year AD 1355 (595 BP) according to the age model (Figure 5a). Higher concentrations of foraminifera in the upper part and higher counts of test linings in the lower part indicate a better preservation and a reduction in dissolution of the carbonate shells after AD 1355. Calculated sedimentation rates show higher rates up to 0.20 cm/yr compared with 0.05 cm/yr below 90 cm (Figure 2). Foraminifera shells were buried faster and thus preserved better from dissolution by ocean waters. Furthermore, the degradation of organic matter within the sediment can decrease the pH of the pore water and affect the preservation of carbonate shells (Jennings and Helgadottir, 1994). Higher grain sizes below 80 cm could have increased pore water fluxes and thus enhanced degradation of organic material.

The foraminifera data show a general decrease in relative temperatures from the onset of the record, at 100 BC, until the minimum values at around AD 1690 (Figure 6e), and suggest a progressive weakening of the IC component in the WGC throughout this interval. This trend is consistent with previous studies from the Disko Bugt area (Andresen et al., 2011; Krawczyk et al., 2016; Lloyd, 2006a; Perner et al., 2011) and is part of a wider atmospheric cooling trend since the Holocene Thermal Maximum at around 6500 yr BP (Dahl-Jensen et al., 1998; Kobashi et al., 2011; Krawczyk et al., 2016; Lloyd et al., 2007; McGregor et al., 2015; Perner et al., 2012; Vinther et al., 2010).

The temperature of the WGC in Disko Bugt was relatively high between 100 BC and AD 450 (Figure 6a) which corresponds well with former studies in the Disko Bugt region (Andresen et al., 2011; Perner et al., 2011, Figure 6d). A diatom-based sea ice reconstruction indicates relatively diminished sea ice at this time (Krawczyk et al., 2013, Figure 6b). This relatively warm time interval correlates with a generally warm period in the Northern Hemisphere, the 'Roman Warm Period' (RWP; lasting 350 BC to AD 300) (e.g. Ljungqvist, 2010; Mann et al., 2009; Figure 6a). It was followed by a marked decrease in relative WGC temperature between AD 400 and 700. This cooling of the WGC is broadly concurrent with onset of the Dark Ages Cold Period (DACP; from AD 300 to 800) in Europe. This is also recorded in Vaigat (Andresen et al., 2011) and was synchronous with a lowering of air temperature as recorded at the ice core at GISP2 in Greenland (Kobashi et al., 2011). However, at AD 700, still within the European DACP, the WGC current and the air temperature on the GISP2 site increased markedly again (Figure 6c). Warm conditions during the DACP have also been recorded in the Irminger Sea proximal to SE Greenland (Andresen et al., 2017) and indicate a highly variable climate with episodic warm conditions in the ocean near SE and W Greenland at this time. During the following period, which corresponds to a period of climatic amelioration in Europe, the 'Medieval Climate Anomaly' (MCA; from AD 800 to 1300) (Ljungqvist, 2010; Mann et al., 2009) and the temperature of the WGC and on the GrIS declined compared with levels during the RWP and maximum values during DACP, but stay relatively high.

A further cooling took place between AD 1400 and 1700 within the cold time period on the Northern hemisphere generally known as the 'LIA' (from AD 1300 to 1900 (Ljungqvist, 2010)). The LIA has been linked with frequently occurring atmospheric blocking situations and negative NAO in response to lowered solar activity (Barriopedro et al., 2008). This atmospheric configuration favours shrinking and westward displacement of the Subpolar Gyre (Barrier et al., 2015) and thus warming of the IC in the vicinity of SE and SW Greenland (Andresen et al., 2012a, 2017; Seidenkrantz et al., 2008). At the same time, the EGC strengthened (Andresen et al., 2012a; Perner et al., 2015); whereas the result was more stratified waters in SE Greenland, it is unclear whether the mixing of these two water masses along W Greenland resulted in an overall warming or cooling of the WGC in Disko Bugt. Our data indicate an overall cooling of the WGC with a minimum during the LIA, occurring from AD 1400–1650, which is concurrent with episodic marked minima in SSTs in the Irminger Sea offshore SE Greenland (Andresen et al., 2017; Perner et al., 2016).

The benthic foraminifera assemblage shows a steady increase in WGC temperature starting at AD 1700. However, the LIA generally terminates around 1900, around 200 years later (Ljungqvist, 2010). A similar trend of late-LIA warming can be observed in records of reconstructed sea ice coverage, which shows decreasing percentages of sea ice indicating diatoms from AD 1650 onwards (Krawczyk et al., 2013). This is explained by a decreased meltwater input and a reduction in the cooling of surface waters. These data somewhat contradict the timing of maximum glacier extent of Jakobshavn Isbræ, which is usually reconstructed to AD 1850 (Briner et al., 2011; Weidick and Bennike, 2007; Young et al., 2011). The air temperature reconstruction from GISP2 (Kobashi et al., 2011), however, shows a strong increase starting around AD 1850. This may indicate a slow response of the Jakobshavn Isbræ terminus to ocean warming and a faster response to changes in air temperatures at this time. The WGC temperature during the 20th century in our study shows the highest percentages (74%) of WWIs throughout the record. CTD measurements at station SJA3 (Figure 1), close to the core location, show a clear warming trend of bottom waters of more than 2°C between 1954 and 2007 (Holland et al., 2008). Results presented here indicate that this dramatic warming is part of a longer warming process that was initiated in AD 1700. Lloyd et al. (2011) correlated these data to foraminiferal assemblage composition as well as to retreat rates of Jakobshavn Isbræ. However, the glacier terminus only started to retreat when WGC temperatures increased to temperatures similar to AD 700 and air temperature also started to rise. Our results demonstrate that the magnitude of recent warming is unprecedented at least in the last 1300 years. Finally, it is interesting to note the strong correlation of our bottom water temperature records with air temperatures recorded 600 km northeast of Disko Bugt at *GISP2* (Figure 6c).

Glaciomarine sedimentation and its links to climatic changes

Sediment supply in the area proximal to marine-terminating glaciers can be characterised by three main processes: suspension settling from meltwater plume discharge, rainout from melting and overturning icebergs and gravity-driven mass movements (Cofaigh et al., 2001; Mugford, 2008). Except for the turbidite between 117 and 121 cm in core ACDC2014-001, we find no further evidence of mass-wasting events in either core and assume that meltwater and IRD sedimentation are the two dominant processes delivering sediment to the core site. The meltwater plume sedimentation of clay and silt is usually highest near the grounding line and decreases exponentially with the distance from the glacier margin (Dowdeswell, 1987).

Icebergs, on the other hand, can transport debris across the grain size spectrum, from clay to boulders, over thousands of kilometres, releasing the material as they melt (Mugford, 2008). Previous studies have shown that variability in IRD deposition in certain Greenland fjords is mainly controlled by variability in the amount of icebergs produced by nearby glaciers (Andresen et al., 2012b; Mugford and Dowdeswell, 2011). However, in certain settings, additional factors may potentially also modulate the amount of IRD deposited. These changes in the melting rate of the icebergs because of ocean and air temperature variability, changes in iceberg transport pathways (route and travel time) because of wind influence and/or changing distance between glacier margin and core site over time as well as changes in the initial sediment load in the ice before calving influenced by mélange persistence and/or growth of glacier tongues (Andresen et al., 2017; Syvitski and

Shaw, 1995). These processes are also kept in mind when interpreting the causes of IRD variability in the two investigated cores. Here, we assume that the influence from potentially variable wind patterns is negligible since Ilulissat Fjord is relatively narrow. Icebergs calved from Jakobshavn Isbræ are channelled directly to the fjord mouth before entering the bay and passing over the core sites as they are entrained in ocean currents (Figure 1).

Our grain size analyses show synchronous sedimentary changes in the two cores situated 6 km apart (Figures 1 and 6), indicating that the changes are spatially homogeneous and represent changes to the amount of icebergs passing over the sites, rather than sporadic localised IRD drop loads. Between the onset of records (75 BC in core ACDC2014-001 and AD 100 in core ACDC2014-003), AD 1400 sedimentation is characterised by relatively high, but gradually decreasing IRD displaying a series of centennial long episodes of increased IRD fluxes.

The gradual decrease in IRD sedimentation from 75 BC to AD 1400 occurs during the general cooling trend in the late Holocene, which culminates in the LIA cold event (Kobashi et al., 2011; Perner et al., 2011) and the readvance of Jakobshavn Isbræ (Briner et al., 2010; Weidick and Bennike, 2007; and others) after AD 1500. The gradual IRD decrease was followed by an interval with almost no IRD deposition from AD 1400 to 1900, indicating that meltwater plume sedimentation was the dominant process at that time. We interpret the marked decrease in IRD at AD 1400 mainly as the result of a reduction in the calving rate of Jakobshavn Isbræ because of a more stable and advanced configuration. Despite the lower flux of IRD, the sedimentation rates increase in that interval (Figure 2), which can be explained by a closer proximity to the glacier front and with this an increase in meltwater plume sedimentation (Dowdeswell, 1987). Moreover, we speculate that under cooling atmospheric temperatures during the transition into the LIA, the ice mélange in Ilulissat Isfjord would have remained coherent most of the time and thus hindered icebergs from exiting Ilulissat Fjord thereby limiting IRD deposition. This process has been proposed for cold periods in East Greenland fjords where little or no IRD deposition is recorded in sediment cores (Dowdeswell and Dowdeswell, 1989). According to Landsat Satellite images of the area show that this process takes place in the Isfjord on seasonal scales today (https://landsatlook.usgs.gov/viewer.html). During winter, the Isfjord is covered in a relative stable ice mélange that breaks up in the summer months causing massive amounts of icebergs to drift into Disko Bugt (Sohn et al., 1998). Sea ice reconstructions from outer Disko Bugt support this hypothesis since high percentages of sea ice–associated diatoms, indicating cooling, are found during times of low IRD sedimentation and vice versa (Figure 6; Krawczyk et al., 2013). A decrease in iceberg production could also have affected the meltwater plume extension, as especially large icebergs floating down the fjord can block the distribution of the plume. The lack of larger icebergs during the LIA, on the other hand, would have enabled the meltwater plume to flow unhindered through the fjord and with this increasing the sedimentation rate at the core sites.

Finally, the lack of IRD from AD 1400 to 1900 may be attributable to an overall decrease in the sediment load of icebergs relating to the formation of a marked floating glacier tongue. Sediment is predominantly entrained into the lowest part of a glacier, close to the glacier bed (Alley et al., 1997; Cuffey et al., 2000; Dowdeswell and Dowdeswell, 1989; Knight, 1997). In its present-day configuration, after the break-up of its floating tongue in 2002 (Joughin et al., 2008; Motyka et al., 2011), icebergs calve from the full depth of the Jakobshavn Isbræ glacier terminus, which includes the sediment-rich basal ice layer (Figure 8). However, when a floating glacier tongue develops, the base of the glacier is exposed to submarine melting prior to calving and thin, tabular, sediment-poor icebergs calve from the tip of the floating tongue. When a floating tongue is present, the majority of coarse

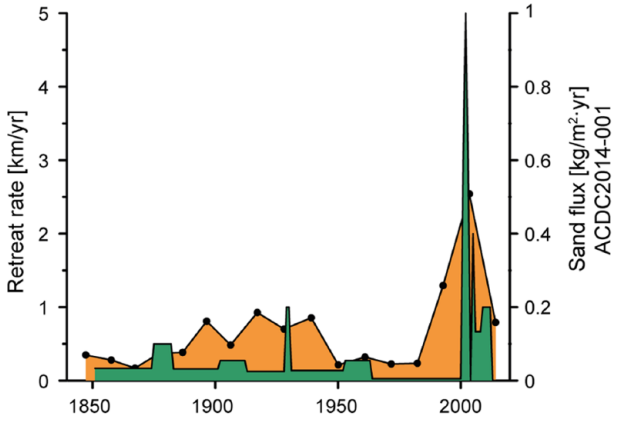

Figure 7. Estimated retreat rates of Jakobshavn Isbræ based on observed glacier front positions (Weidick and Bennike, 2007) underlain by the sand flux rates in the respective time periods.

sediment is deposited close to the grounding line of the glacier (in the fjord) and is not entrained in icebergs (Domack and Harris, 1998). Besides a decreased calving rate and the strengthening of the ice mélange during the LIA, it is possible that decreased air temperatures may have promoted the formation of a glacier tongue at the terminus of Jakobshavn Isbræ, akin to the major outlets in northern Greenland today which experience high-Arctic conditions (low temperatures, low precipitation) and similar to the hypothesis of an ice tongue at Helheim Glacier in SE Greenland lasting until the end of the LIA (Andresen et al., 2017). This could explain the absence of IRD after AD 1400. Historical observations of relatively 'ice-free' conditions in the Isfjord in the early 1700s (see Weidick and Bennike, 2007, for a summary) may indicate the presence of a floating glacier tongue for a time, rather than a calving tidewater front. Indeed, the terminus of Jakobshavn Isbræ forms a small floating tongue during winter even today (Amundson et al., 2010; Das et al., 2008), suggesting that even slight climatic cooling would promote the formation of a glacier tongue. Accepting this theory, our data indicate that a floating glacier tongue may have developed at the terminus of Jakobshavn Isbræ between AD 1500 and 1600. This corresponds to the oldest estimations of glacier extent on land from Young et al. (2011) and contradicts the estimations from Briner et al. (2011) about a late Jakobshavn Isbræ advance most likely around AD 1800.

The increase in IRD flux from the middle of the 19th century coincides with the documented retreat of Jakobshavn Isbræ (Figure 7). Between AD 1880 and 1940, higher IRD fluxes and higher retreat rates are calculated. This is followed by a period from 1940 until the 1990s where retreat rates were low and deposition of IRD decreases significantly. Both peak again around AD 2000 with unprecedented retreat rates and the highest IRD flux rates in the past 500 years.

Warm water influence and other drivers on IRD sedimentation

To assess the forcing behind Jakobshavn Isbræ activity during the latest 2000 years, we compare the glaciological data with proxy data of oceanic and climatic changes. The overall variability in the abundance of warm water foraminifera resembles the variability in iceberg rafting over the past 2000 years in both cores (Figure 6). This suggests that, over multi-decadal to centennial timescales, there is a connection between warm water inflow and the configuration and calving regime of Jakobshavn Isbræ. It is noticeable that the high warm water inflow between AD 0 and 400 is concurrent with three major peaks in the calculated IRD flux at AD 100, 250 and 400 (Figure 6d and e).

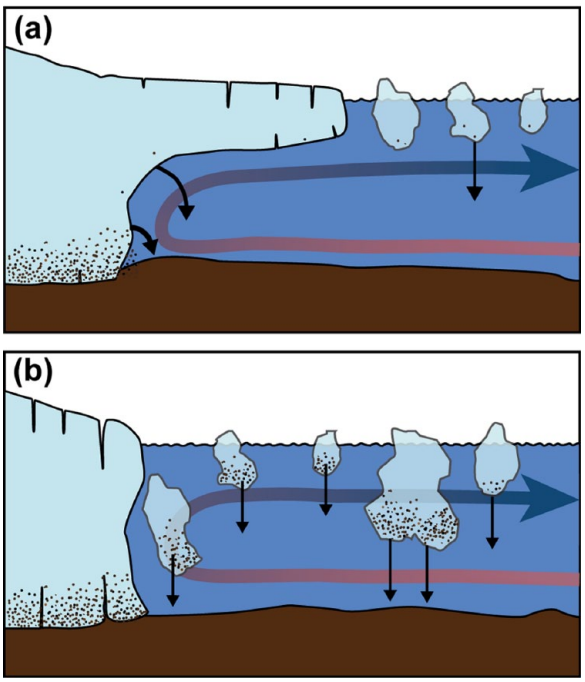

Figure 8. Conceptual figure of sediment load in icebergs depending on the presence (a) or absence (b) of a floating glacier tongue. Black arrows indicate pathways of sediment deposition. The red/blue arrows represent the current circulation in the fjord system.

Despite the period of relatively cold bottom water and air temperatures between AD 450 and 600 (Figure 6c), the IRD flux stays relatively high. However, there are no major peaks in either core during that time, suggesting no major calving or 'break-up' events. The strong warming around AD 700 does not directly affect the IRD record. However, the highest flux rates in core ACDC2014-003 and a smaller peak in core ACDC2014-001 can be identified shortly after (AD ~770). Between 7500 cal. yr BP and AD 1500, the glacier terminus was located behind its current position (Young et al., 2011). Our data suggest that Jakobshavn Isbræ was configured as a calving glacier at this time and that IRD peaks reflect increased iceberg calving caused by increased warm water inflow. The absence of a floating glacier tongue results in a high sediment load in icebergs (Figure 8b), which may explain the generally high flux rates from the onset of the record until AD 1100. Between 1100 and AD 1500, both IRD and WGC temperatures are relatively low and declining, which likely reflects the early onset of the LIA cooling. The short but prominent warming around AD 1400 is not linked with an increase in IRD deposition, which could be explained by the initiated growth of a glacier tongue as regional temperatures cooled towards their LIA minima. This glaciodynamic response to cooling may also explain the lower amplitude of IRD fluxes since AD 1850 compared with the older part of the core, where flux rates are more than three times as high as modern values. It is noticeable that even if warming of the WGC had commenced already in AD 1700, it was only as the relative temperature matched that before AD 700 and air temperatures started to rise that the glacier started to retreat around AD 1850. The retreat (Figure 7) resulted in the disintegration of the floating ice tongue in 2002 (Joughin et al., 2008; Motyka et al., 2011). This may indicate that, in the absence of a glacier tongue, IRD deposition in Disko Bugt might increase dramatically in the near future and is therefore simply not captured yet in seafloor sediment records.

Statistical analyses of the grain size data were performed to identify possible drivers in the IRD record (Supplementary Figure 2, available online). In core ACDC2014-001, a strong cyclicity with a period of ~150 years was found from the starting point of the periodogram around AD 440 until AD 650 (95% significance). This almost coincides with an interval between 450 BC and AD 250 where the sun's 150-yr cycle was unusually strong (Knudsen et al., 2009). This cyclicity could not be confirmed by core ACDC2014-003, in which a strong cyclicity with a peak period undulating between 180 and 210 years was identified throughout the record. This periodicity is close to the Suess (de Vriess) solar cycle with a dominant periodicity around 210 years (Damon and Sonett, 1991). The presence of solar-like cyclicities in the two records indicates that solar activity might be one possible factor influencing the timing of some of the variations in IRD sedimentation, but it is not possible to identify solar variability as a dominant driver of changes at the two core sites. Rather, the record of IRD abundance appears to reflect multiple factors including the variations in oceanographic conditions, like temperature and sea-ice coverage, but also the position of the glacier front and changes in the configuration and calving style of Jakobshavn Isbræ.

Conclusion

In the early part of the record between 80 BC and AD 400, the data indicate high WGC temperatures resulting in high fluxes of IRD sedimentation. Similar to other records in Disko Bugt region, this period is followed by large fluctuations in temperature during the timing of the DACP. A general cooling trend from AD 700 reduced the calving activity of Jakobshavn Isbræ indicated by decreasing IRD sedimentation leading into a period of almost no IRD within the sediment. We interpret this signal as a direct indicator of a floating glacier tongue around AD 1500. Due to the presence of a floating glacier tongue IRD deposition stayed low, WGC temperature started to rise again in AD 1700. We show that the instrumentally measured warming since the beginning of the 20th century is part of a long-term warming trend starting 200 years earlier. However, the documented retreat of the glacier terminus starting in AD 1850 was not initiated until WGC temperatures were matching temperatures from 1400 years ago combined with rising air temperatures at that time. WGC temperatures over the past 2000 years correspond well with other palaeo-oceanographic reconstructions from outer Disko Bugt, the Vaigat Strait as well as with reconstructed air temperatures on the GrIS. The IRD deposition, derived from Jakobshavn Isbræ, follows the general trend of WGC temperature but the sedimentation process does not react instantaneously. We conclude that the sedimentary record in the vicinity of Jakobshavn Isbræ is influenced by a complex variety of glaciological and climatic factors. This includes the presence of an ice tongue, an extended duration of coherent winter mélange, the proximity and retreat rates of the glacier front as well as the production rate of icebergs.

Acknowledgements

We thank the captain and crew of the R/V Porsild for crucial help during fieldwork. Thanks also to Christina Rosenberg Lynge, Pernille Stockmarr, Wendy Freeman-Roth and Glenn Oxfeldt Jensen for helping during the labwork. Finally, we thank Anders Anker Bjørk for helpful discussions. Finally, we want to thank the anonymous reviewer for helpful and constructive comments.

Funding

The project 'Past and future dynamics of the Greenland Ice Sheet: what is the ocean hiding?' is funded by the VILLUM Foundation (grant no. 10100).

ORCID iD

David J Wangner https://orcid.org/0000-0002-3042-4598

References

Alley RB, Andrews JT, Brigham-Grette J et al. (2010) History of the Greenland Ice Sheet: Paleoclimatic insights. *Quaternary Science Reviews* 29(15–16): 1728–1756.

Alley RB, Cuffey KM, Evenson EB et al. (1997) How glaciers entrain and transport basal sediment: Physical constraints. *Quaternary Science Reviews* 16: 1017–1038.

Amundson JM, Fahnestock M, Truffer M et al. (2010) Ice mélange dynamics and implications for terminus stability, Jakobshavn Isbræ, Greenland. *Journal of Geophysical Research: Earth Surface* 115(F1): F01005.

Andresen CS, Hansen MJ, Seidenkrantz M-S et al. (2012a) Mid- to late-Holocene oceanographic variability on the Southeast Greenland shelf. *The Holocene* 23(2): 167–178.

Andresen CS, Kokfelt U, Sicre M-A et al. (2017) Exceptional 20th century glaciological regime of a major SE Greenland outlet glacier. *Scientific Reports* 7(1): 13626.

Andresen CS, McCarthy DJ, Dylmer CV et al. (2011) Interaction between subsurface ocean waters and calving of the Jakobshavn Isbræ during the late Holocene. *The Holocene* 21(2): 211–224.

Andresen CS, Straneo F, Ribergaard MH et al. (2012b) Rapid response of Helheim Glacier in Greenland to climate variability over the past century. *Nature Geoscience* 5(1): 37–41.

Andersen OGN (1981) The annual cycle of temperature, salinity, currents and water masses in Disko Bugt and adjacent waters, West Greenland. *Biosciences* 5: 1–36.

Bamber JL, Griggs JA, Hurkmans RTWL et al. (2013) A new bed elevation dataset for Greenland. *The Cryosphere* 7(2): 499–510.

Barrier N, Deshayes J, Treguier A-M et al. (2015) Heat budget in the North Atlantic subpolar gyre: Impacts of atmospheric weather regimes on the 1995 warming event. *Progress in Oceanography* 130: 75–90.

Barriopedro D, García-Herrera R and Huth R (2008) Solar modulation of Northern Hemisphere winter blocking. *Journal of Geophysical Research* 113(D14): D14118.

Beaird N, Straneo F and Jenkins W (2017) Characteristics of meltwater export from Jakobshavn Isbræ and Ilulissat Icefjord. *Annals of Glaciology* 58: 107–117.

Bindschadler RA (1984) Jakobshavns Glacier drainage basin: A balance assessment. *Journal of Geophysical Research* 89(C2): 2066–2072.

Blaauw M and Christen JA (2011) Flexible paleoclimate age-depth models using an autoregressive gamma process. *Bayesian Analysis* 6(3): 457–474.

Box JE (2002) Survey of Greenland instrumental temperature records: 1873-2001. *International Journal of Climatology* 22(15): 1829–1847.

Box JE and Colgan W (2013) Greenland Ice Sheet mass balance reconstruction. Part III: Marine ice loss and total mass balance (1840–2010). *Journal of Climate* 26(18): 6990–7002.

Box JE, Yang L, Bromwich DH et al. (2009) Greenland Ice Sheet surface air temperature variability: 1840–2007. *Journal of Climate* 22: 4029–4049.

Briner JP, Stewart HAM, Young NE et al. (2010) Using proglacial-threshold lakes to constrain fluctuations of the Jakobshavn Isbræ ice margin, western Greenland, during the Holocene. *Quaternary Science Reviews* 29(27–28): 3861–3874.

Briner JP, Young NE, Thomas EK et al. (2011) Varve and radiocarbon dating support the rapid advance of Jakobshavn Isbræ during the Little Ice Age. *Quaternary Science Reviews* 30(19–20): 2476–2486.

Carr SJ and Hiemstra JF (2013) Sedimentary evidence against a local ice-cap on the Shetland Isles at the Last Glacial Maximum. *Proceedings of the Geologists Association* 124(3): 484–502.

Chen JL, Wilson CR and Tapley BD (2006) Satellite gravity measurements confirm accelerated melting of Greenland Ice Sheet. *Science* 313: 1958–1960.

Cofaigh CÓ, Dowdeswell JA and Grobe H (2001) Holocene glacimarine sedimentation, inner Scoresby Sund, East Greenland: The influence of fast-flowing ice-sheet outlet glaciers. *Marine Geology* 175: 103–129.

Cooper MA, Michaelides K, Siegert MJ et al. (2016) Paleofluvial landscape inheritance for Jakobshavn Isbræ catchment, Greenland. *Geophysical Research Letters* 43: 6350–6357.

Corbett LB, Young NE, Bierman PR et al. (2011) Paired bedrock and boulder 10Be concentrations resulting from early Holocene ice retreat near Jakobshavn Isfjord, western Greenland. *Quaternary Science Reviews* 30(13–14): 1739–1749.

Csatho B, Schenk T, Van Der Veen CJ et al. (2008) Intermittent thinning of Jakobshavn Isbræ, West Greenland, since the Little Ice Age. *Journal of Glaciology* 54(184): 131–144.

Cuffey KM, Conway H, Gades AM et al. (2000) Entrainment at cold glacier beds. *Geology* 28(4): 351–354.

Dahl-Jensen D, Mosegaard K, Gundestrup N et al. (1998) Past temperatures directly from the Greenland Ice Sheet. *Science* 282(5387): 268–271.

Damon PE and Sonett CP (1991) Solar and terrestrial components of the atmospheric C-14 variation spectrum. In: Sonett MS, Giampapa MS and Matthews MS (eds) *The Sun in Time*. Tucson, AZ: University of Arizona Press, pp. 360–388.

Das SB, Joughin I, Behn MD et al. (2008) Fracture propagation to the base of the Greenland Ice Sheet during supraglacial lake drainage. *Science* 320: 778–781.

Domack E and Harris P (1998) A new depositional model for ice shelves, based upon sediment cores from the Ross Sea and the MacRobertson shelf, Antarctica. *Annals of Glaciology* 27: 281–284.

Dowdeswell JA (1987) Processes of glacimarine sedimentation. *Progress in Physical Geography* 11: 52–90.

Dowdeswell JA and Dowdeswell EK (1989) Debris in icebergs and rates of glaci-marine sedimentation: Observations from Spitsbergen and a simple model. *Journal of Geology* 97(2): 221–231.

Enderlin EM, Howat IM and Vieli A (2013) High sensitivity of tidewater outlet glacier dynamics to shape. *The Cryosphere* 7(3): 1007–1015.

Enderlin EM, Howat IM, Jeong S et al. (2014) An improved mass budget for the Greenland Ice Sheet. *Geophysical Research Letters* 41(3): 866–872.

Hammer Ø, Harper DAT and Ryan PD (2001) PAST: Paleontological statistics software package for education and data analysis. *Palaeontologia Electronica* 4(1): 5–7.

Hogan KA, Dowdeswell JA and Cofaigh ÓC (2012) Glacimarine sedimentary processes and depositional environments in an embayment fed by West Greenland ice streams. *Marine Geology* 311–314: 1–16.

Holland DM, Thomas RH, de Young B et al. (2008) Acceleration of Jakobshavn Isbræ triggered by warm subsurface ocean waters. *Nature Geoscience* 1(10): 659–664.

Jakobsson M, Mayer L, Coakley B et al. (2012) The International Bathymetric Chart of the Arctic Ocean (IBCAO) version 3.0. *Geophysical Research Letters* 39: L12609.

Jennings AE and Helgadottir G (1994) Foraminiferal assemblages from the fjords and shelf of eastern Greenland. *Journal of Foraminiferal Research* 24(2): 123–144.

Jennings AE and Weiner NJ (1996) Environmental change in eastern Greenland during the last 1300 years: Evidence from foraminifera and lithofacies in Nansen Fjord, 68 N. *The Holocene* 6(2): 179–191.

Jennings AE, Andrews JTÓ, Cofaigh C et al. (2017) Ocean forcing of Ice Sheet retreat in central west Greenland from LGM to the early Holocene. *Earth and Planetary Science Letters* 472: 1–13.

Jennings AE, Knudsen KL, Hald M et al. (2002) A mid-Holocene shift in Arctic sea-ice variability on the East Greenland Shelf. *The Holocene* 12(1): 49–58.

Joughin I, Abdalati W and Fahnestock M (2004) Large fluctuations in speed on Greenland's Jakobshavn Isbræ glacier. *Nature* 432(7017): 608–610.

Joughin I, Howat IM, Fahnestock M et al. (2008) Continued evolution of Jakobshavn Isbræ following its rapid speedup. *Journal of Geophysical Research: Earth Surface* 113: F04006.

Juggins S (2007) User guide C2 software for ecological and palaeoecological data analysis and visualisation (User Guide Version 15). Available at: https://www.staff.ncl.ac.uk/stephen.juggins/software/code/C2.pdf.

Kelley SE, Briner JP and Young NE (2013) Rapid ice retreat in Disko Bugt supported by ^{10}Be dating of the last recession of the western Greenland Ice Sheet. *Quaternary Science Reviews* 82: 13–22.

Kjeldsen KK, Korsgaard NJ, Bjørk AA et al. (2015) Spatial and temporal distribution of mass loss from the Greenland Ice Sheet since AD 1900. *Nature* 528: 396–400.

Knight PG (1997) The basal layer of glaciers and ice sheets. *Quaternary Science Reviews* 16: 975–993.

Knudsen MF, Riisager P, Jacobsen BH et al. (2009) Taking the pulse of the Sun during the Holocene by joint analysis of 14C and10Be. *Geophysical Research Letters* 36(16): 3–7.

Kobashi T, Kawamura K, Severinghaus JP et al. (2011) High variability of Greenland surface temperature over the past 4000 years estimated from trapped air in an ice core. *Geophysical Research Letters* 38: L21501.

Krawczyk DW, Witkowski A, Lloyd J et al. (2013) Late-Holocene diatom derived seasonal variability in hydrological conditions off Disko Bay, West Greenland. *Quaternary Science Reviews* 67: 93–104.

Krawczyk DW, Witkowski A, Moros M et al. (2016) Quantitative reconstruction of Holocene sea ice and sea surface temperature off West Greenland from the first regional diatom data set. *Paleoceanography* 31(1): 1–23.

Ljungqvist FC (2010) A new reconstruction of temperature variability in the extra-tropical northern hemisphere during the last two millennia. *Geografiska Annaler: Series A, Physical Geography* 92(3): 339–351.

Lloyd JM (2006a) Late-Holocene environmental change in Disko Bugt, west Greenland: Interaction between climate, ocean circulation and Jakobshavn Isbrae. *Boreas* 35(1): 35–49.

Lloyd JM (2006b) Modern distribution of benthic foraminifera from Disko Bugt, West Greenland. *Journal of Foraminiferal Research* 36(4): 315–331.

Lloyd JM, Kuijpers A, Long A et al. (2007) Foraminiferal reconstruction of mid- to late-Holocene ocean circulation and climate variability in Disko Bugt, West Greenland. *The Holocene* 17(8): 1079–1091.

Lloyd JM, Moros M, Perner K et al. (2011) A 100 yr record of ocean temperature control on the stability of Jakobshavn Isbrae, West Greenland. *Geology* 39(9): 867–870.

Lloyd JM, Park LA, Kuijpers A et al. (2005) Early Holocene palaeoceanography and deglacial chronology of Disko Bugt, West Greenland. *Quaternary Science Reviews* 24(14–15): 1741–1755.

Lomb NR (1976) Least-squares frequency analysis of unequally spaced data. *Astrophysics and Space Science* 39(2): 447–462.

McGregor HV, Evans MN, Goosse H et al. (2015) Robust global ocean cooling trend for the pre-industrial Common Era. *Nature Geoscience* 8(9): 671–677.

McMillan M, Leeson A, Shepherd A et al. (2016) A high resolution record of Greenland mass balance. *Geophysical Research Letters* 43: 7002–7010.

Mann ME, Zhang Z, Rutherford S et al. (2009) Global signatures and dynamical origins of the Little Ice Age and Medieval Climate Anomaly. *Science* 326(5957): 1256–1260.

Meischner D and Rumohr J (1974) A light-weight, high-momentum gravity corer for subaqueous sediments. *Senckenbergiana Maritima* 6(1): 105–117.

Moros M, Lloyd JM, Perner K et al. (2016) Surface and sub-surface multi-proxy reconstruction of middle to late Holocene palaeoceanographic changes in Disko Bugt, West Greenland. *Quaternary Science Reviews* 132: 146–160.

Motyka RJ, Truffer M, Fahnestock M et al. (2011) Submarine melting of the 1985 Jakobshavn Isbræ floating tongue and the triggering of the current retreat. *Journal of Geophysical Research: Earth Surface* 116: F01007.

Mugford RI (2008) *Numerical Modelling of Sediment Delivery from Tidewater Glaciers to the Marine Environment*. Cambridge: University of Cambridge.

Mugford RI and Dowdeswell JA (2011) Modeling glacial meltwater plume dynamics and sedimentation in high-latitude fjords. *Journal of Geophysical Research: Earth Surface* 116: F01023.

Myers PG, Kulan N and Ribergaard MH (2007) Irminger water variability in the West Greenland Current. *Geophysical Research Letters* 34: L17601.

Ouellet-Bernier M-M, de Vernal A, Hillaire-Marcel C et al. (2014) Paleoceanographic changes in the Disko Bugt area, West Greenland, during the Holocene. *The Holocene* 24(11): 1573–1583.

Perner K, Jennings AE, Moros M et al. (2016) Interaction between warm Atlantic-sourced waters and the East Greenland Current in northern Denmark Strait (68°N) during the last 10,600 cal a BP. *Journal of Quaternary Science* 31(5): 472–483.

Perner K, Moros M, Jennings AE et al. (2013) Holocene palaeoceanographic evolution off West Greenland. *The Holocene* 23(3): 374–387.

Perner K, Moros M, Lloyd JM et al. (2011) Centennial scale benthic foraminiferal record of late Holocene oceanographic variability in Disko Bugt, West Greenland. *Quaternary Science Reviews* 30: 2815–2826.

Perner K, Moros M, Lloyd JM et al. (2015) Mid to late Holocene strengthening of the East Greenland Current linked to warm subsurface Atlantic water. *Quaternary Science Reviews* 129: 296–307.

Pritchard HD, Arthern RJ, Vaughan DG et al. (2009) Extensive dynamic thinning on the margins of the Greenland and Antarctic ice sheets. *Nature* 461: 971–975.

Reimer P, Bard E, Bayliss A et al. (2013) IntCal13 and Marine13 radiocarbon age calibration curves 0–50,000 years cal BP. *Radiocarbon* 55(4): 1869–1887.

Ribeiro S, Moros M, Ellegaard M et al. (2012) Climate variability in West Greenland during the past 1500 years: Evidence from a high-resolution marine palynological record from Disko Bay. *Boreas* 41(1): 68–83.

Ribergaard MH, Kliem N and Jespersen M (2006) *HYCOM for the North Atlantic Ocean with special emphasis on West Greenland Waters*. DMI-Technical Report 06-07, 1–31.

Rignot E and Kanagaratnam P (2006) Changes in the Velocity Structure of the Greenlance Ice Sheet. *Science* 311: 986–990.

Rignot E, Fenty I, Menemenlis D et al. (2012) Spreading of warm ocean waters around Greenland as a possible cause for glacier acceleration. *Annals of Glaciology* 53(60): 257–266.

Scargle JD (1982) Studies in astronomical time series analysis. II: Statistical aspects of spectral analysis of unevenly spaced data. *Astrophysical Journal* 263: 835–853.

Schulz M and Mudelsee M (2002) REDFIT: Estimating red-noise spectra directly from unevenly spaced paleoclimatic time series. *Computers & Geosciences* 8(3): 421–426.

Schumann K, Völker D and Weinrebe WR (2012) Acoustic mapping of the Ilulissat Ice Fjord mouth, West Greenland. *Quaternary Science Reviews* 40: 78–88.

Seidenkrantz MS, Roncaglia L, Fischel A et al. (2008) Variable North Atlantic climate seesaw patterns documented by a late Holocene marine record from Disko Bugt, West Greenland. *Marine Micropaleontology* 68(1–2): 66–83.

Sha L, Jiang H, Seidenkrantz MS et al. (2014) A diatom-based sea-ice reconstruction for the Vaigat Strait (Disko Bugt, West Greenland) over the last 5000 yr. *Palaeogeography, Palaeoclimatology, Palaeoecology* 403: 66–79.

Sheldon CM, Jennings AE, Andrews JTÓ et al. (2016) Ice stream retreat following the LGM and onset of the west Greenland current in Uummannaq Trough, west Greenland. *Quaternary Science Reviews* 45: 1–20.

Sheldon CM, Seidenkrantz M-S, Frandsen P et al. (2015) Variable influx of West Greenland Current water into the Labrador Current through the last 7200 years: A multiproxy record from Trinity Bay (NE Newfoundland). *Arktos* 1(8): 1–19.

Shepherd A, Ivins ER, Geruo A et al. (2012) A reconciled estimate of Ice-Sheet Mass Balance. *Science* 338(6111): 1183–1189.

Sohn H-G, Jezek KC and van der Veen CJ (1998) Jakobshavn Glacier, west Greenland: 30 years of spaceborne observations. *Geophysical Research Letters* 25(14): 2699–2702.

Straneo F and Heimbach P (2013) North Atlantic warming and the retreat of Greenland's outlet glaciers. *Nature* 504: 36–43.

Straneo F, Curry RG, Sutherland DA et al. (2011) Impact of fjord dynamics and glacial runoff on the circulation near Helheim Glacier. *Nature Geoscience* 4(5): 322–327.

Straneo F, Heimbach P, Sergienko O et al. (2013) Challenges to understanding the dynamic response of Greenland's marine terminating glaciers to oceanic and atmospheric forcing. *Bulletin of the American Meteorological Society* 94(8): 1131–1144.

Straneo F, Sutherland DA, Holland D et al. (2012) Characteristics of ocean waters reaching Greenland's glaciers. *Annals of Glaciology* 53(60): 202–210.

Streuff KÓ, Cofaigh C, Hogan K et al. (2017) Seafloor geomorphology and glacimarine sedimentation associated with fast-flowing ice sheet outlet glaciers in Disko Bay, West Greenland. *Quaternary Science Reviews* 169: 206–230.

Syvitski JPM and Shaw J (1995) Sedimentology and geomorphology of fjords. *Geomorphology and Sedimentology of Estuaries* 53: 113–178.

Van den Broeke MR, Enderlin EM, Howat IM et al. (2016) On the recent contribution of the Greenland ice sheet to sea level change. *The Cryosphere* 10(5): 1933–1946.

Vinther BM, Andersen KK, Jones PD et al. (2006) Extending Greenland temperature records into the late eighteenth century. *Journal of Geophysical Research Atmospheres* 111: D11105.

Vinther BM, Jones PD, Briffa KR et al. (2010) Climatic signals in multiple highly resolved stable isotope records from Greenland. *Quaternary Science Reviews* 29(3–4): 522–538.

Weidick A and Bennike O (2007) *Quaternary Glaciation History and Glaciology of Jakobshavn Isbræ and the Disko Bugt Region, West Greenland: A Review*. Copenhagen: Geological Survey of Denmark and Greenland Bulletin.

Wessel P, Smith WHF, Scharroo R et al. (2013) Generic mapping tools: Improved version released. *Eos, Transactions American Geophysical Union* 94(45): 409–410.

Young NE, Briner JP, Stewart HAM et al. (2011) Response of Jakobshavn Isbræ, Greenland, to Holocene climate change. *Geology* 39(2): 131–134.